Red emitting, cucurbituril-capped, pH-responsive conjugated oligomer-based nanoparticles for drug delivery and cellular imaging

*Jousheed Pennakalathil,[a,b] Ermira Jahja[c], E. Sıla Özdemir, Özlen Konu,[*c] Dönüs Tuncel[*a,b]*

[a] *Department of Chemistry, Bilkent University, 06800 Ankara, Turkey.*

[b] *Institute of Materials Science and Nanotechnology, National Nanotechnology Research Center (UNAM), Bilkent University, Ankara, 06800, Turkey.*

[c] *Department of Molecular Biology and Genetics, Bilkent University, 06800 Ankara, Turkey.*

Supporting Information

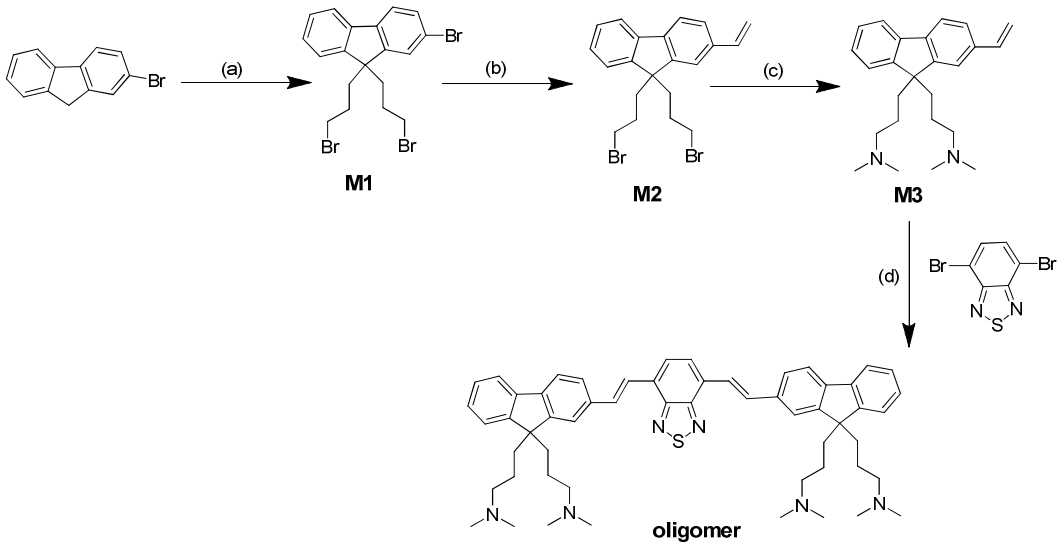

Scheme S1. Synthetic route to oligomer.

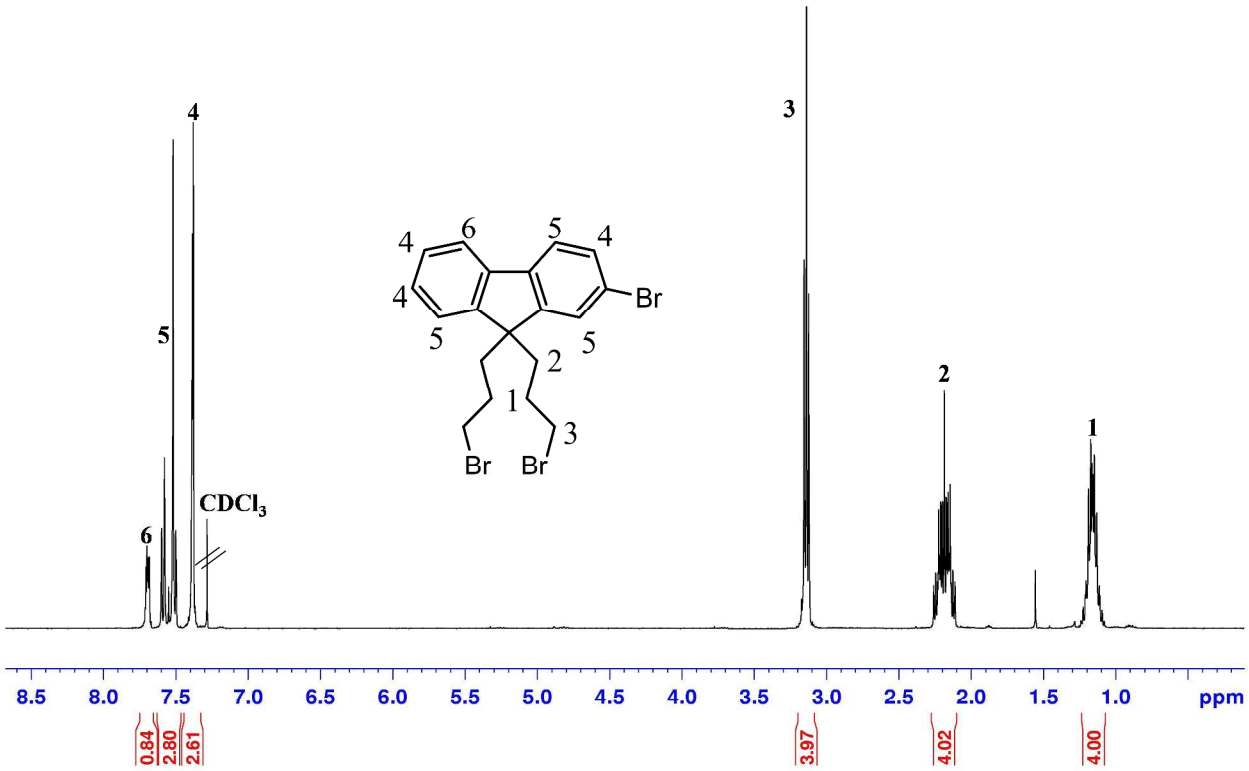

Figure S1. ^{1}H NMR ($CDCl_3$, 400 MHz, 25 °C) spectrum of 2-bromo-9,9-bis(3-bromopropyl)-9H-fluorene, **M1**.

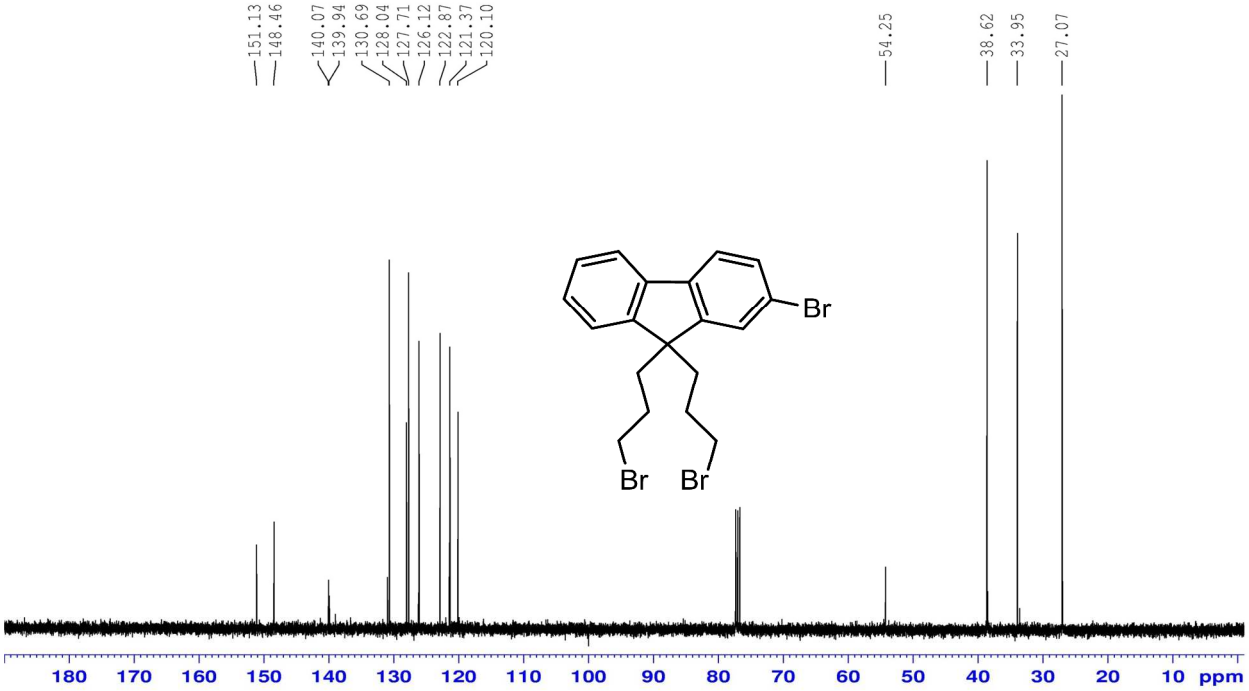

Figure S2. ^{13}C-NMR ($CDCl_3$, 100 MHz, 25 °C) spectrum of 2-bromo-9,9-bis(3-bromopropyl)-9H-fluorene, **M1**.

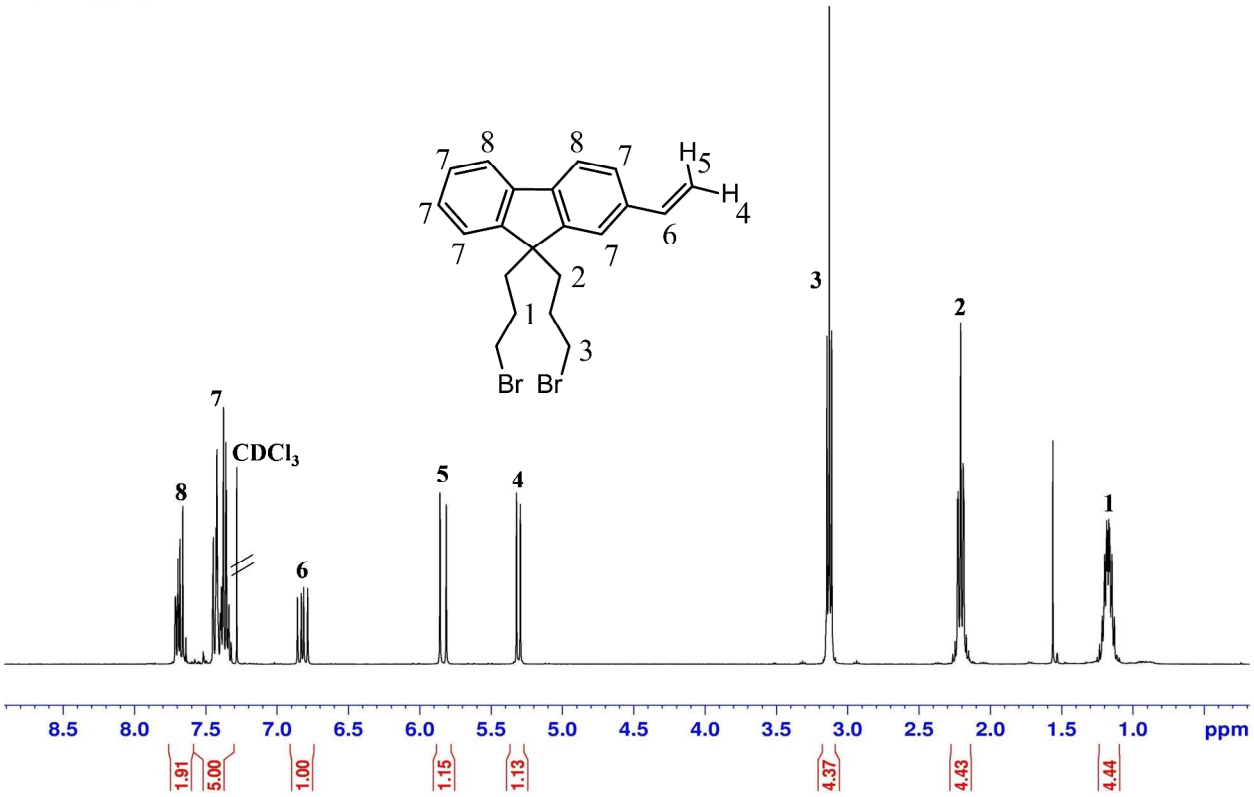

Figure S3. ^{1}H NMR ($CDCl_3$, 400 MHz, 25 °C) spectrum of 9,9-bis(3-bromopropyl)-2-vinyl-9H-fluorene, **M2**.

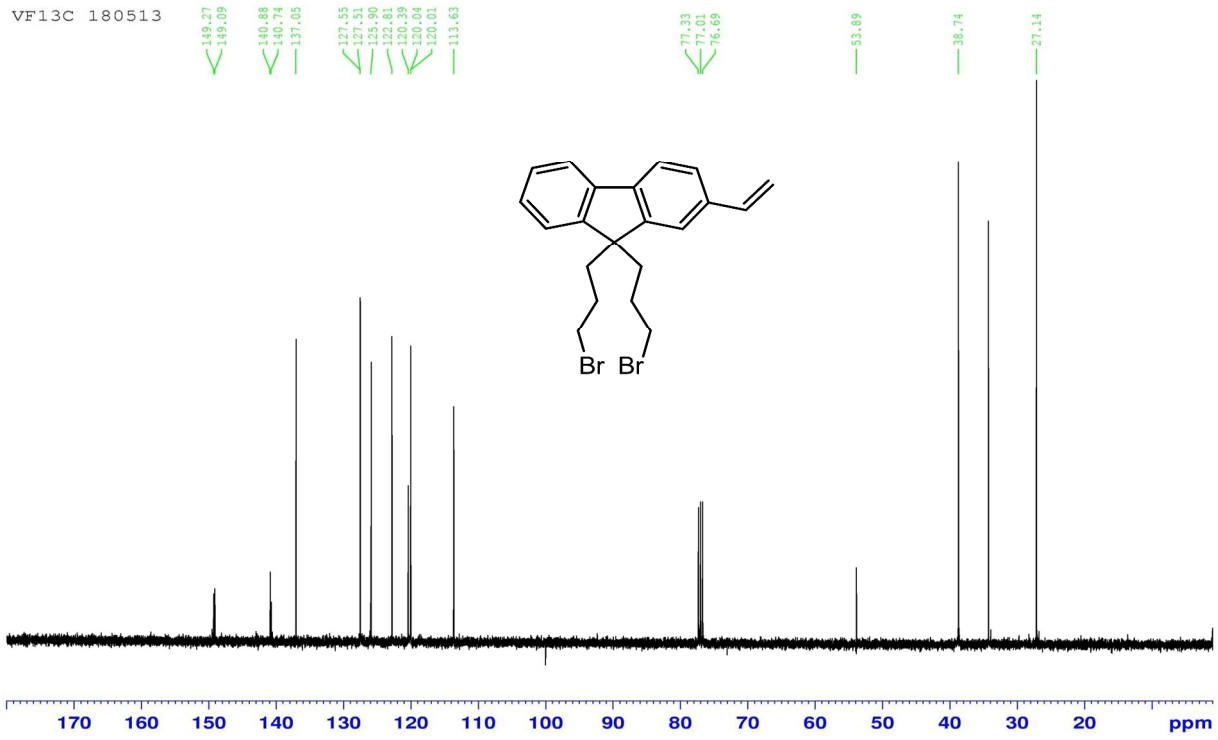

Figure S4. 13C NMR ($CDCl_3$, 100 MHz, 25 °C)spectrum of 9,9-bis(3-bromopropyl)-2-vinyl-9H-fluorene, **M2**.

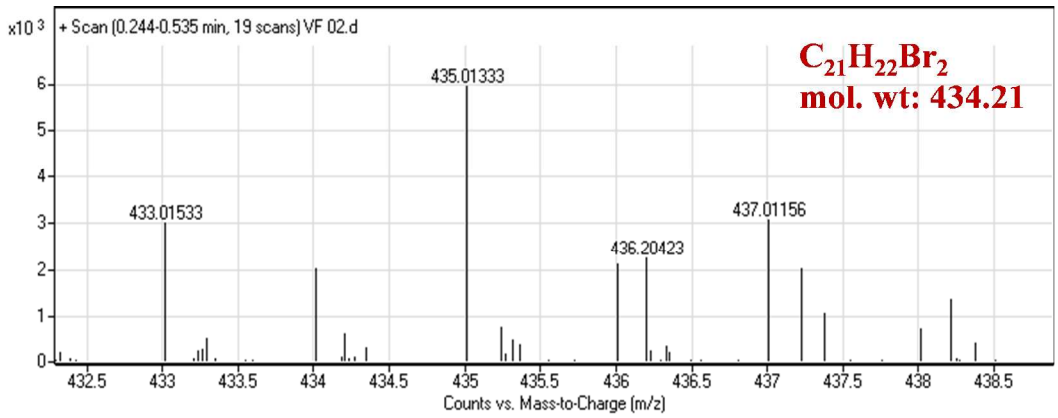

Figure S5. Mass spectrum of 9,9-bis(3-bromopropyl)-2-vinyl-9H-fluorene, **M2**.

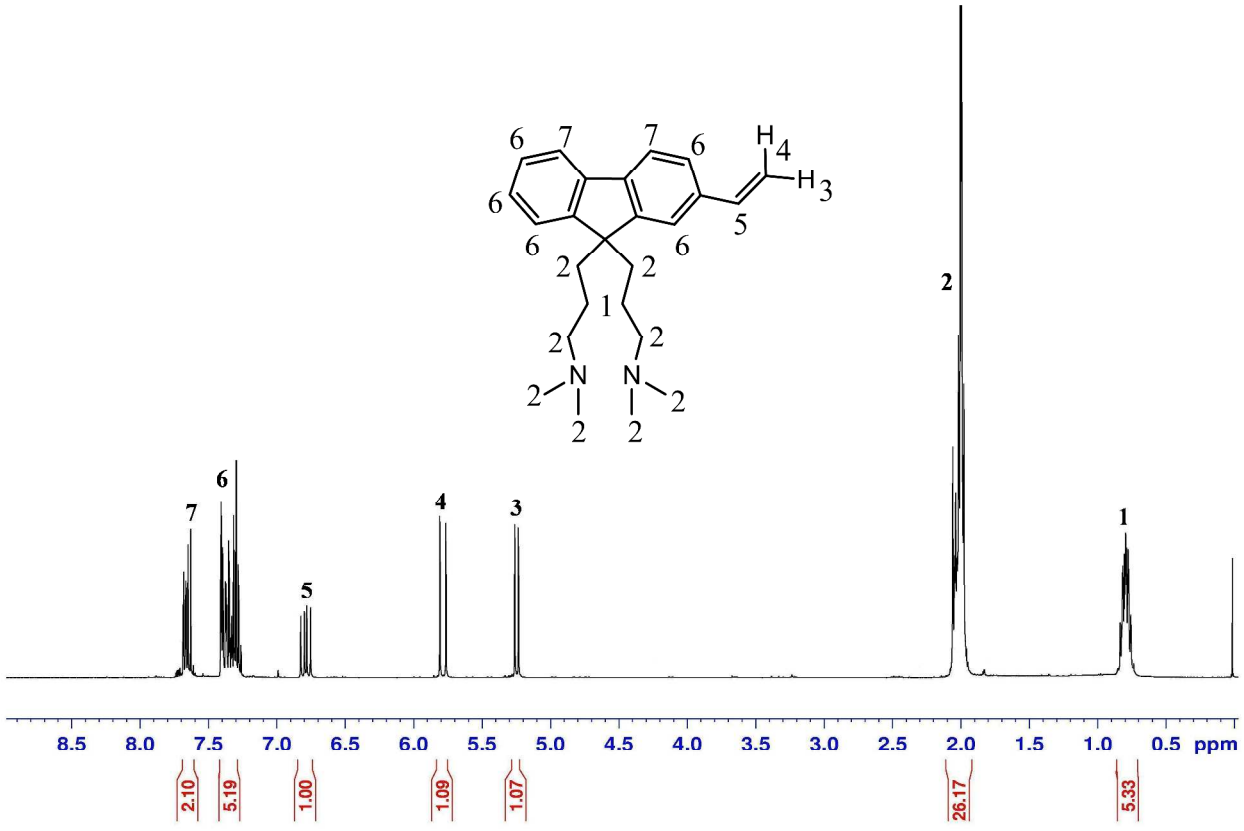

Figure S6. ^1H NMR ($CDCl_3$, 400 MHz, 25 °C) spectrum of 3,3'-(2-vinyl-9H-fluorene-9,9-diyl)bis(N,N-dimethylpropan-1-amine), **M3**.

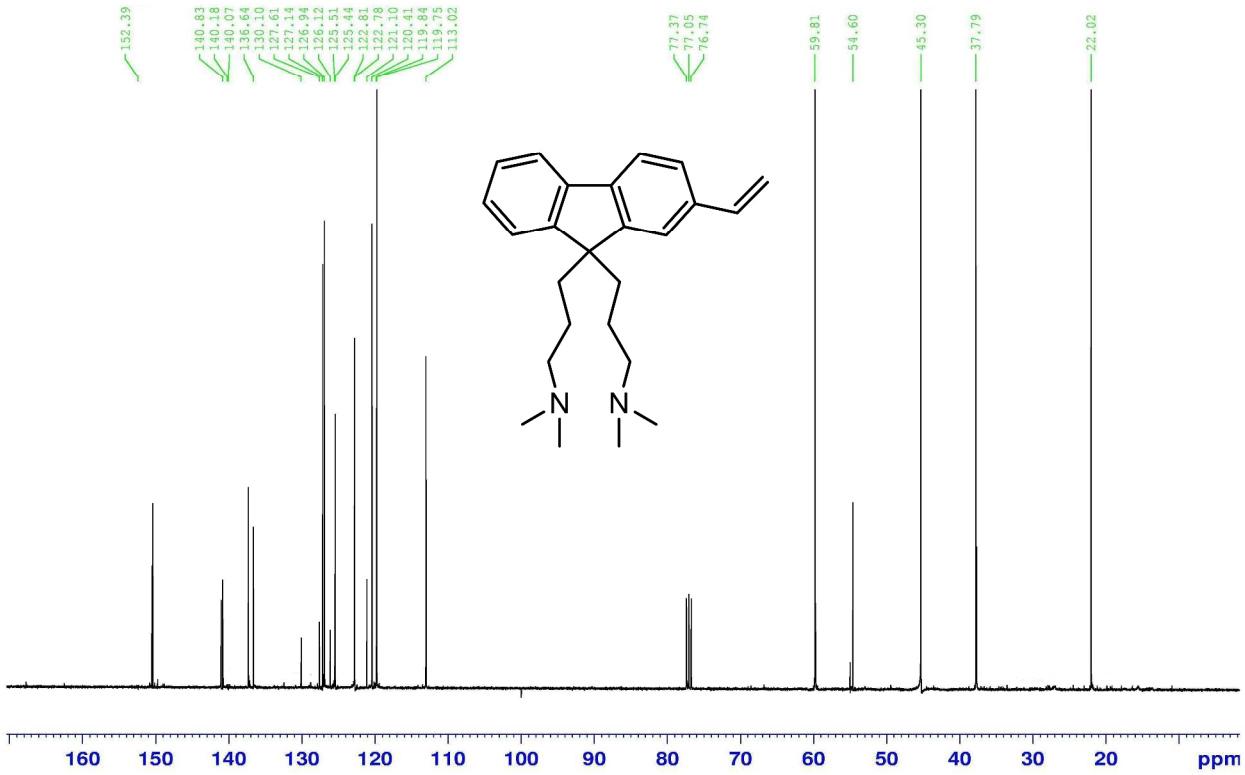

Figure S7. ^{1}H NMR ($CDCl_3$, 400 MHz, 25 °C) spectrum of 3,3'-(2-vinyl-9H-fluorene-9,9-diyl)bis(N,N-dimethylpropan-1-amine), **M3**.

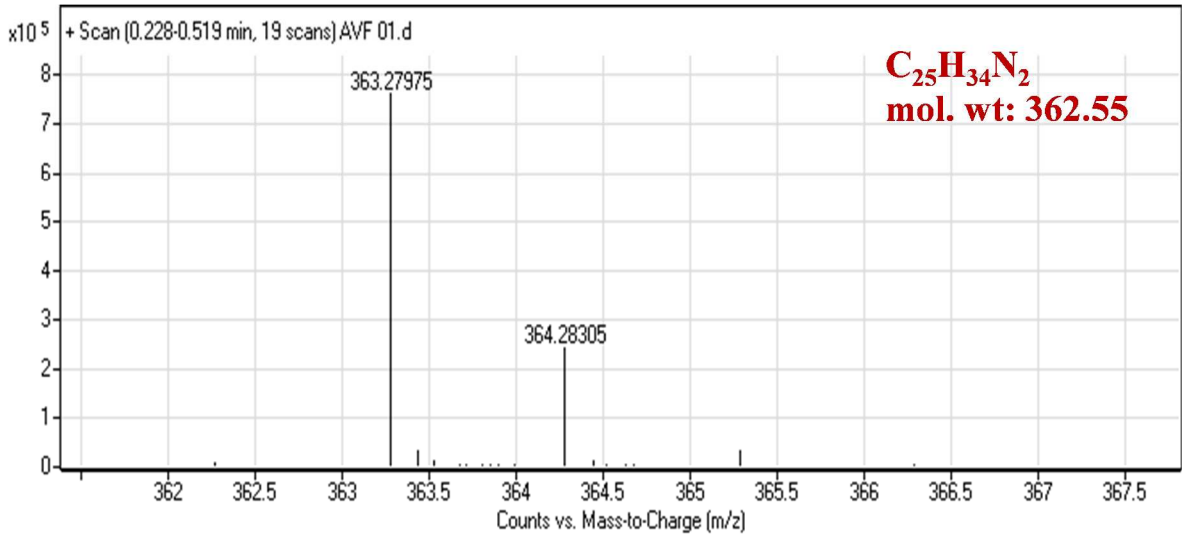

Figure S8. Mass spectrum of 3,3'-(2-vinyl-9H-fluorene-9,9-diyl)bis(N,N-dimethylpropan-1-amine), **M3**.

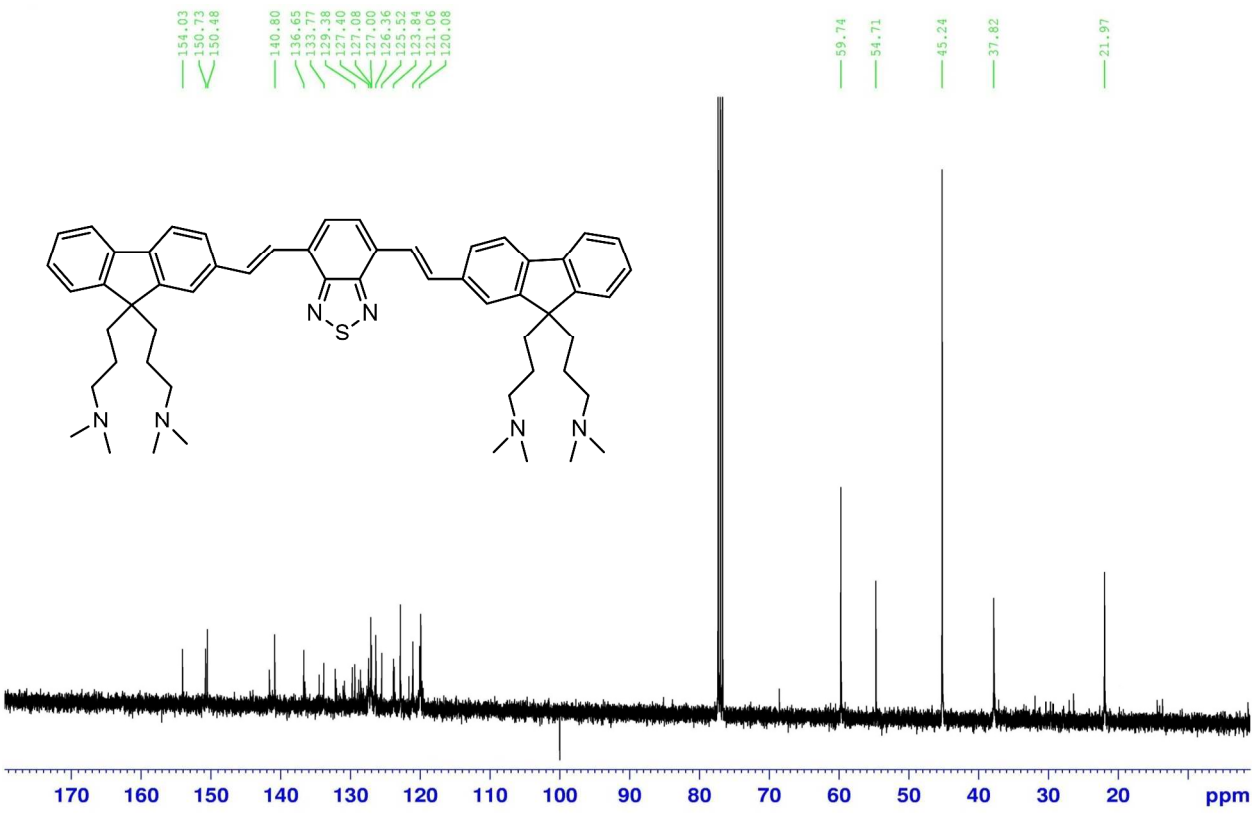

Figure S9. ^{13}C NMR ($CDCl_3$, 100 MHz, 25 °C) spectrum of oligomer.

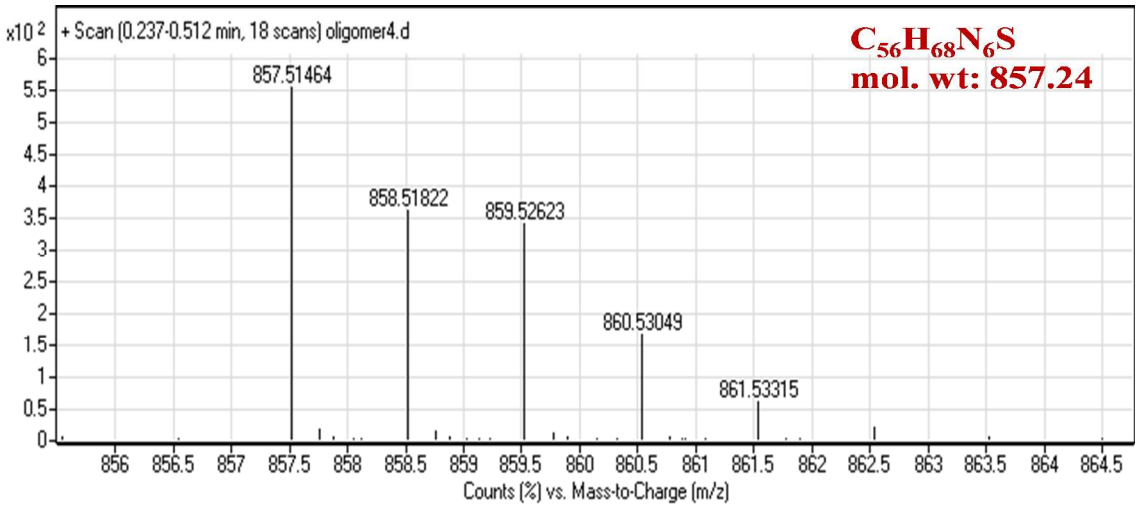

Figure S10. Mass spectrum of oligomer.

Table S1. Z-average size, PDI and zeta potential of oligomer nanoparticles with different concentrations of oligomer solution.

Sl. No.	Con. of oligomer (in THF)	Z-average size (nm)	Average PDI	Zeta potential (mV)
1	1 mg/mL	49.0 ± 0.3	0.23 ± 0.02	21.0 ± 2.4
2	2 mg/mL	50.6 ± 0.6	0.03 ± 0.08	46.2 ± 3.0
3	3 mg/mL	53.4 ± 0.7	0.16 ± 0.04	48.8 ± 4.2
4	4 mg/mL	57.0 ± 0.7	0.19 ± 0.03	52.5 ± 1.3
5	5 mg/mL	90.8 ± 1.0	0.12 ± 0.01	57.2 ± 2.6

		Diam. (nm)	% Intensity	Width (nm)
Z-Average (d.nm): 49.03	Peak 1:	57.28	100.0	28.26
PdI: 0.241	Peak 2:	0.000	0.0	0.000
Intercept: 0.953	Peak 3:	0.000	0.0	0.000

Result quality : Good

		Mean (mV)	Area (%)	Width (mV)
Zeta Potential (mV): 21,7	Peak 1:	21,7	100,0	9,54
Zeta Deviation (mV): 9,54	Peak 2:	0,00	0,0	0,00
Conductivity (mS/cm): 0,208	Peak 3:	0,00	0,0	0,00

Result quality : Good

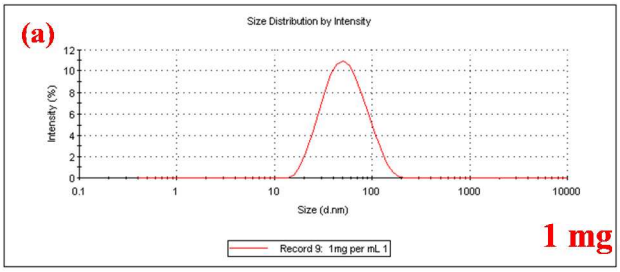

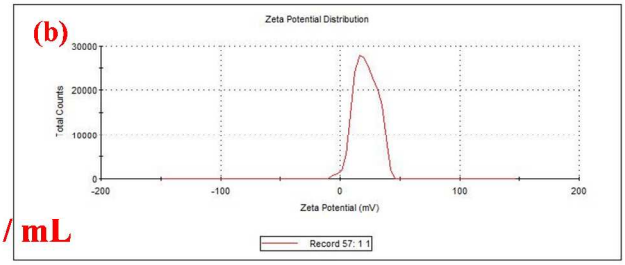

1 mg / mL

		Diam. (nm)	% Intensity	Width (nm)
Z-Average (d.nm): 48.61	Peak 1:	50.32	100.0	17.85
PdI: 0.227	Peak 2:	0.000	0.0	0.000
Intercept: 0.958	Peak 3:	0.000	0.0	0.000

Result quality : Good

		Mean (mV)	Area (%)	Width (mV)
Zeta Potential (mV): 45,1	Peak 1:	48,2	99,0	4,74
Zeta Deviation (mV): 12,4	Peak 2:	3,08	1,0	0,22
Conductivity (mS/cm): 0,0225	Peak 3:	0,00	0,0	0,00

Result quality : Good

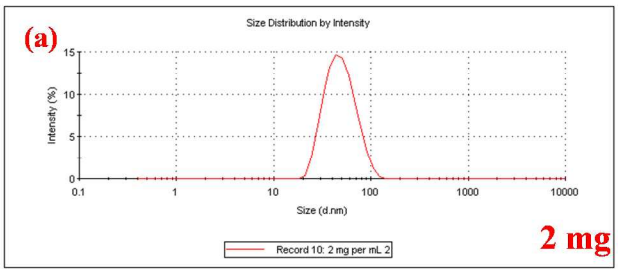

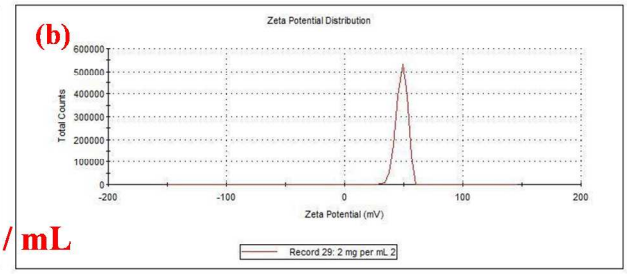

2 mg / mL

		Diam. (nm)	% Intensity	Width (nm)
Z-Average (d.nm): 54.10	Peak 1:	58.72	100.0	21.30
PdI: 0.150	Peak 2:	0.000	0.0	0.000
Intercept: 0.959	Peak 3:	0.000	0.0	0.000

Result quality : Good

		Mean (mV)	Area (%)	Width (mV)
Zeta Potential (mV): 46,6	Peak 1:	46,6	100,0	5,40
Zeta Deviation (mV): 5,40	Peak 2:	0,00	0,0	0,00
Conductivity (mS/cm): 0,0147	Peak 3:	0,00	0,0	0,00

Result quality : Good

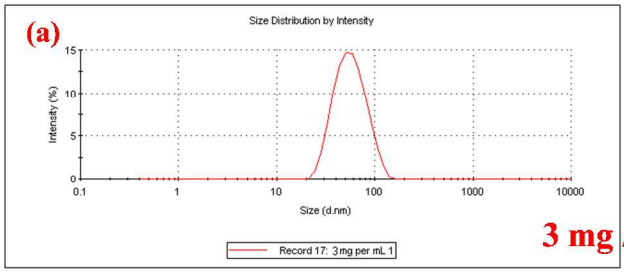

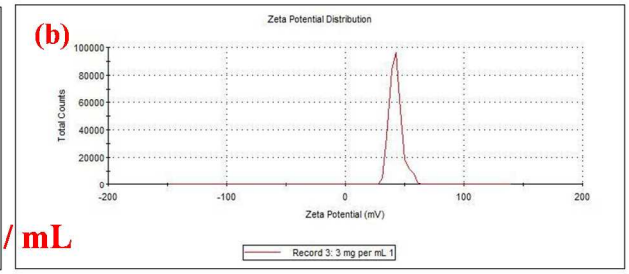

3 mg / mL

		Diam. (nm)	% Intensity	Width (nm)
Z-Average (d.nm): 57.20	Peak 1:	71.63	100.0	35.44
PdI: 0.210	Peak 2:	0.000	0.0	0.000
Intercept: 0.962	Peak 3:	0.000	0.0	0.000

Result quality : Good

		Mean (mV)	Area (%)	Width (mV)
Zeta Potential (mV): 53,8	Peak 1:	53,8	100,0	10,6
Zeta Deviation (mV): 5,2	Peak 2:	0,00	0,0	0,00
Conductivity (mS/cm): 0,0418	Peak 3:	0,00	0,0	0,00

Result quality : Good

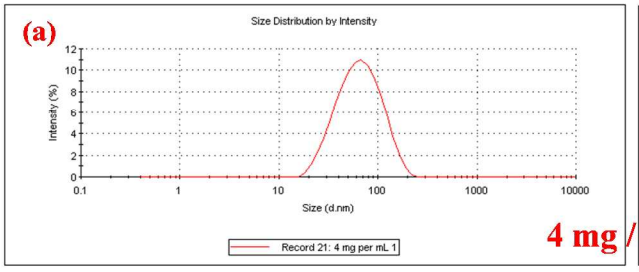

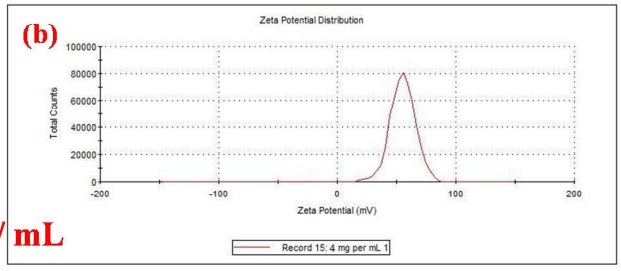

4 mg / mL

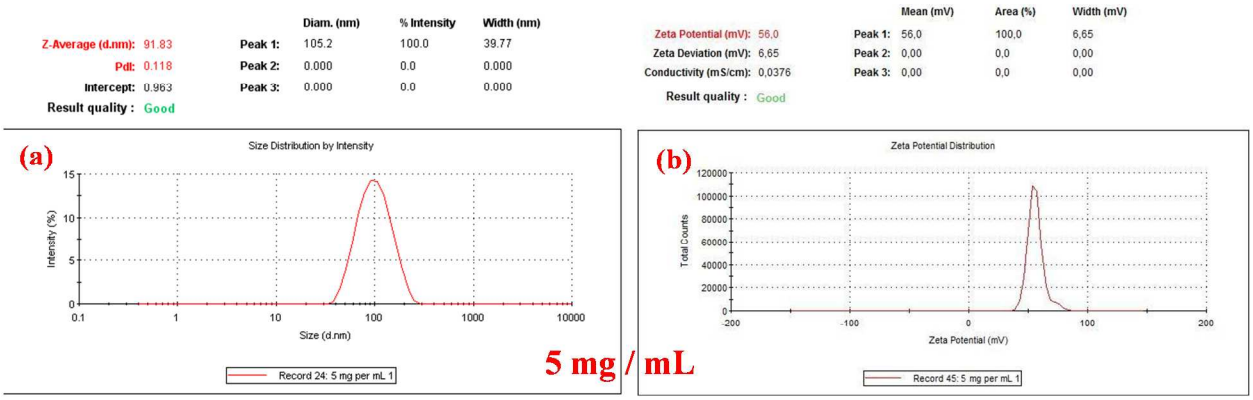

Figure S11. DLS histograms for (a) hydrodynamic size and (b) zeta potential of oligomer nanoparticles with different concentrations of oligomer.

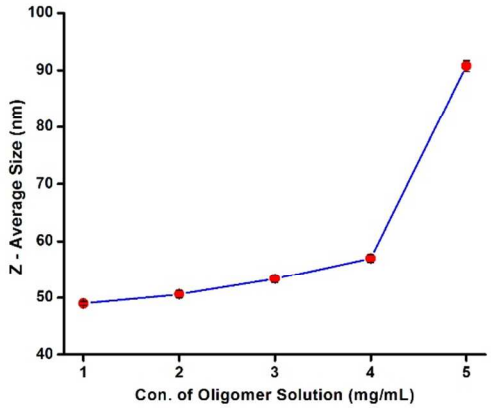

Figure S12. Z-average size vs concentration of oligomer solution (mg/mL THF) of oligomer nanoparticles.

pH sensitivity of oligomer nanoparticles

The pH sensitivity of the oligomer nanoparticles was studied by fluorescence spectroscopy. pH of the dispersion of nanoparticles in water was 6.42 and it was adjusted between 2.30 and 12.50 either by con. HCl or 1M NaOH solution. Emission intensity of fresh nanoparticles dispersion was found to be 115 (ie. at pH = 6.42) and it was gradually increased by increase of pH and reached a maximum value of 455 at pH = 12.50. Similarly, the emission intensity was gradually decreased from 115 by decrease of pH and reached a minimum value of 58 at pH = 2.30. But the nanoparticles were slowly precipitated below the pH = 4.0. Figure S13 shows the fluorescence

spectrum of oligomer nanoparticles in different pH between 2.30 and 12.50. Furthermore, the pH sensitivity of the oligomer nanoparticle was found to be reversible for at least 5 cycles. The reversibility of the pH sensitivity was studied by recording the emission intensity at 615 nm by changing the pH of nanoparticles dispersion from 5.50 to 12.50 and vice versa. The pH sensitivity of the oligomer nanoparticles can be explained by the partial positive charge of the nanoparticle in water. Zeta potential of nanoparticles was found to be +52.5 ± 1.3.

Most probably the changes in the optical properties of oligomer both due to inter and intra-chain interaction as well as the solvent polarity. We observe a decrease in the fluorescent intensity upon converting oligomer into nanoparticles but we also observe a significant decrease in the fluorescent intensity of oligomer when treated with aqueous solution of HCl at pH lower than 5.

Once amine groups are completely protonated, the oligomer chains will be more exposed to highly polar environment.

In the basic pH, the partial positive charges on the surface of the nanoparticle are neutralized by hydroxyl ions and this, in turn, might restrict the interaction of nanoparticles with polar aqueous environment. As a result, an increase in the fluorescent intensity can be observed.

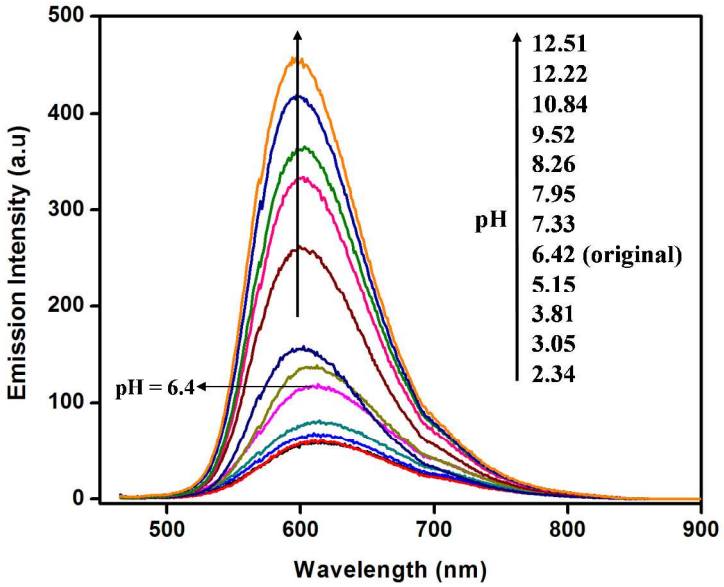

Figure S13. Fluorescence spectrum of oligomer nanoparticle by changing its pH in between 2.50 and 12.50.

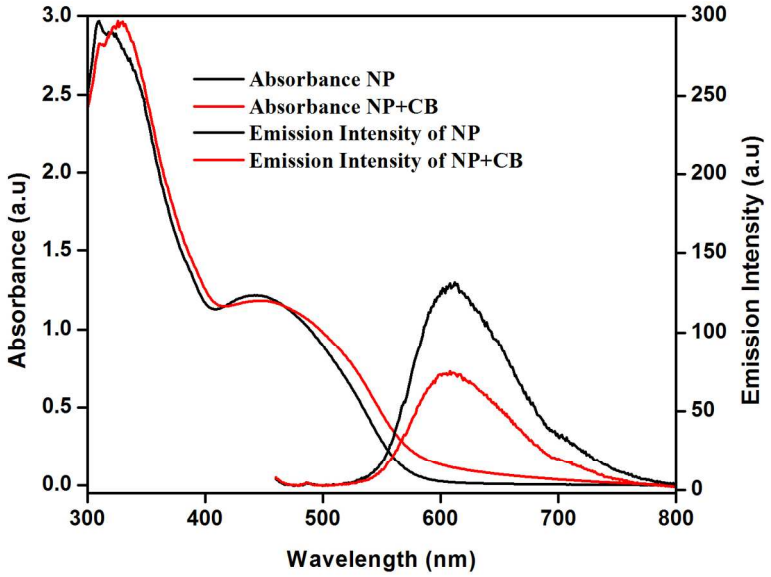

Figure S14. UV-Vis absorbance and fluorescence spectra of oligomer nanoparticles with and without capping CB.

Table S2. The concentrations of camptothecin (CPT), nanoparticle (NP) and cucurbit(7)uril (CB7) used for MTT assays conducted for measuring relative cell viability.

Sample/Concentrations(uM)	**Conc. 1**	**Conc. 2**	**Conc. 3**	**Conc. 4**
CPT	0.125	0.5	2	8
NP	2.15	8.6	34.4	137.6
CB	8.6	34.4	137.6	550.4
NP+CPT	2.15/0.125	8.6/0.5	34.4/2	137.6/8
NP+CB	2.15/8.6	8.6/34.4	34.4/137.6	137.6/550.4
NP+CPT+CB	2.15/0.125/8.6	8.6/0.5/34.4	34.4/2/137.6	137.6/8/550.4
DMSO	0.088	0.467	1.4	2.8

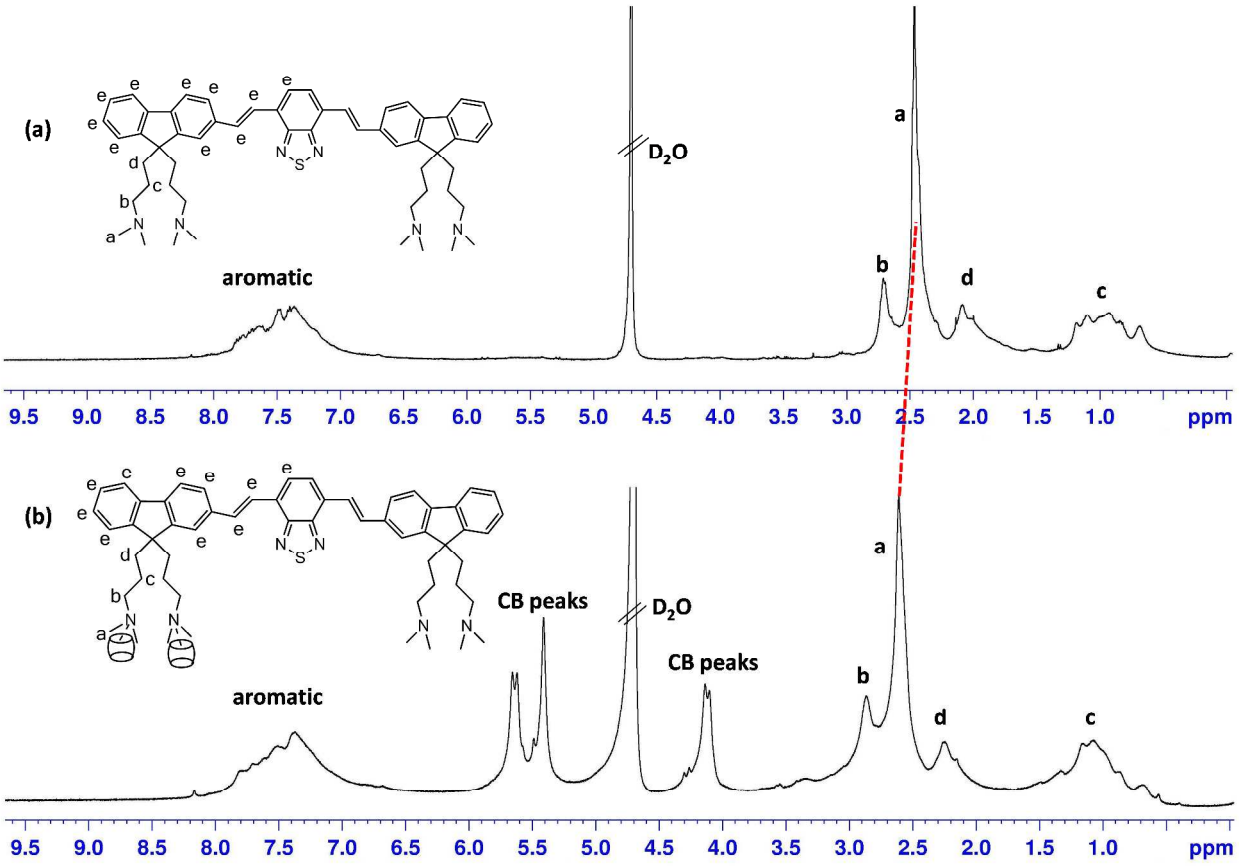

Figure S15: NMR spectra of oligomer NPs (a) without CB addition and (b) with 4.0 equivalents of CB7 (D_2O, 400 MHz, RT).

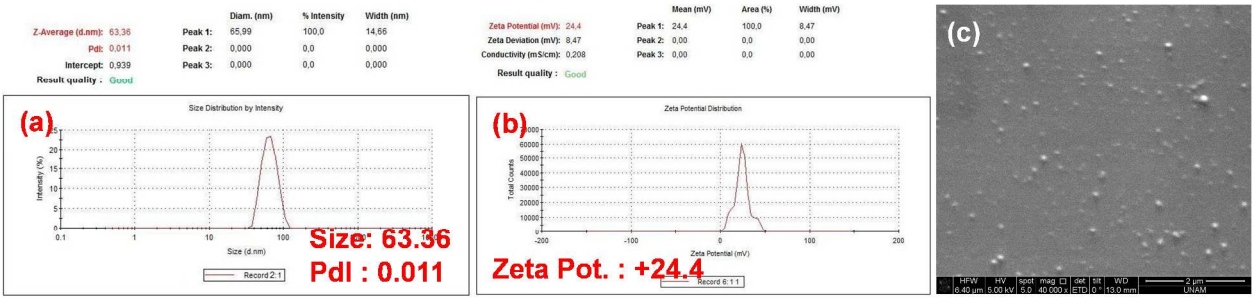

Figure S16: DLS data (a) zeta average size (b) zeta potential and (c) SEM image of CB capped oligomer nanoparticles.

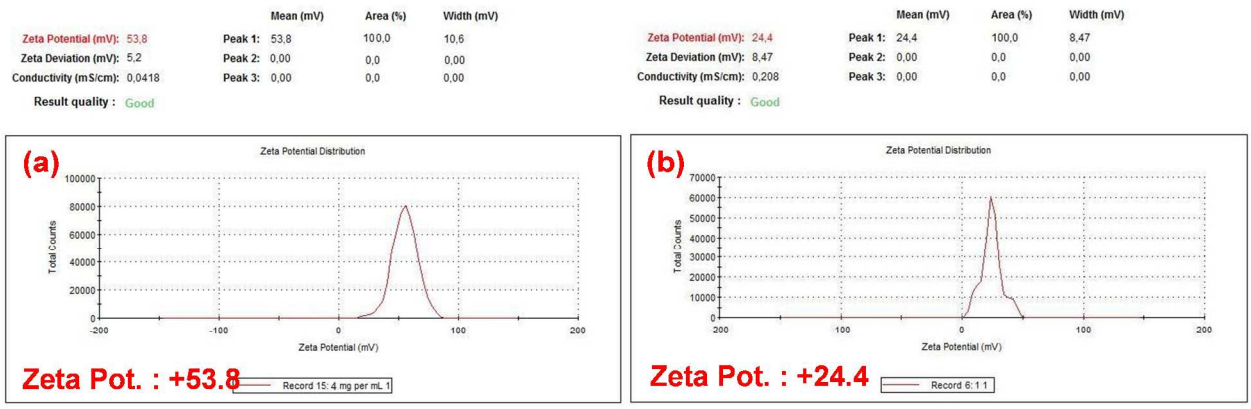

Figure S17: Zeta potential of Oligomer nanoparticles without (a) and with (b) 4 equivalents of CB7 addition.

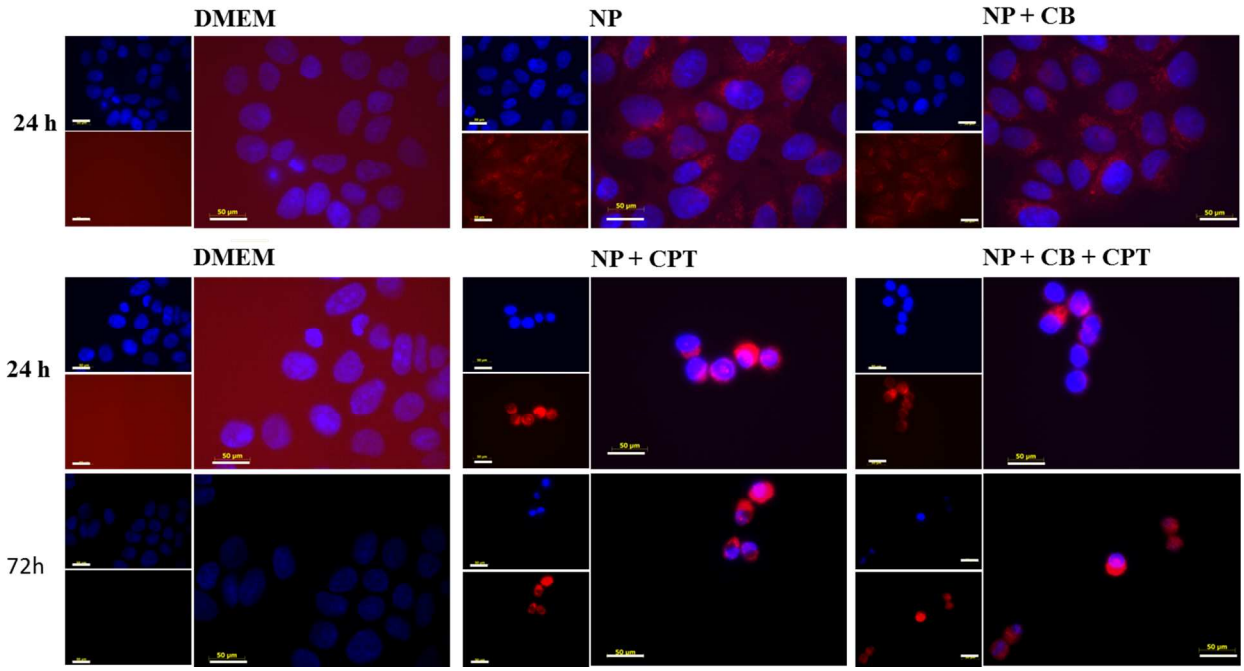

Figure S18: Representative images for MCF7 cells exposed to NP or NP+CB in the absence or presence of camptothecin (CPT) for 24h and 72h in comparison with DMEM control groups. Nuclei were stained with DAPI (blue; LP420) while emission from nanoparticles were obtained using LP590 red filter; and images from all two channels were overlaid (Axio Imager A1, Zeiss; 100X). Scale bars are 50 µm.